The morphology of fluvial-tidal dunes

Prokocki, E. W.; Best, J. L.; Perillo, M. M.; Ashworth, P. J.; Parsons, D. R.; Sambrook-Smith, Greg; Nicholas, A. P.; Simpson, C. J.

DOI:
10.1002/esp.5364

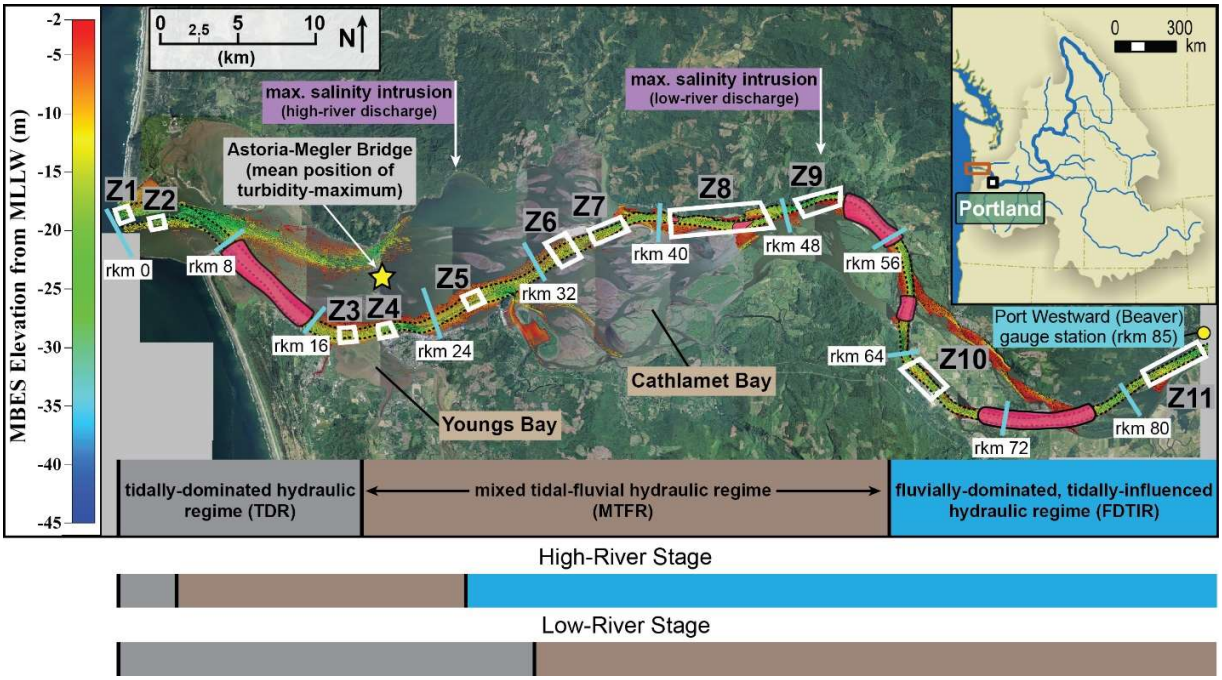

FIGURE 1 Image of the lower Columbia River (LCR) study reach complete with 2007-2011 multi-beam echo sounding (MBES) data coverage of its main channel (dashed black line) provided by the National Oceanographic and Atmospheric Agency (NOAA). Included are: (a) the eleven zones where dune metrics were measured (z1-z11; open white rectangles), (b) the mean longitudinal channel extents of the three major fluvial-tidal hydraulic regimes as defined by Jay et al. (1990) as well as their inferred boundaries during high- and low- river stages (below the figure), (c) the upstream limits of salinity intrusion during high-and low- fluvial flows as reported by Fox et al. (1984) and Chawla et al. (2008), and (d) channel reaches most impacted by dredging of the federal navigation channel between 2005-2010 (pink rectangles). Elevations represent those from the Mean Lower Low Water (MLLW) level at the NOAA Astoria, OR, tide station (ID: 9439040). Refer to Figures 5-8 for magnified images of zones 1-11. Aerial image from US National Agriculture Imagery Program (NAIP) at https://gdg.sc.egov.usda.gov/.

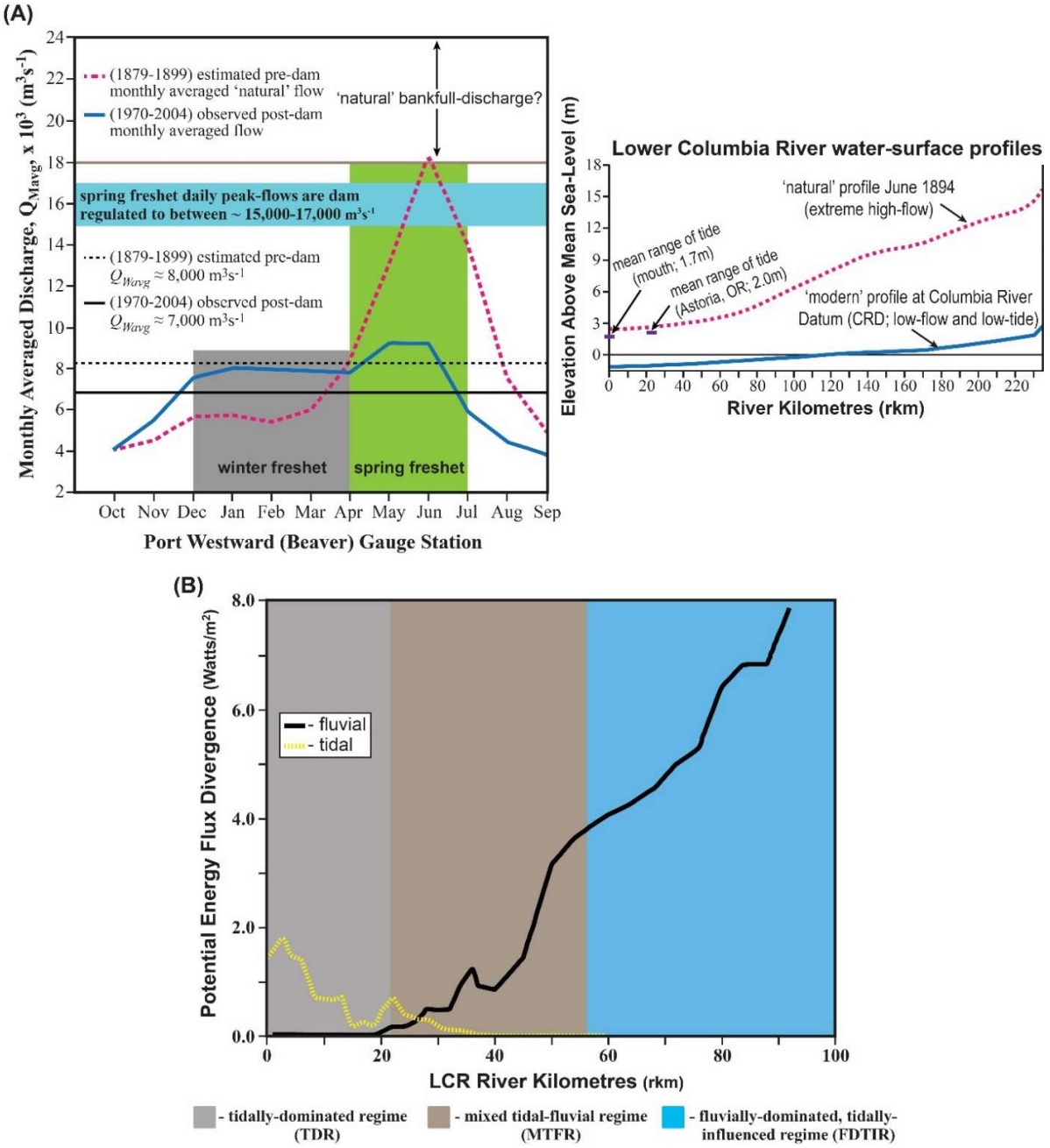

FIGURE 2 (A) Monthly averaged Lower Columbia River 'natural' (1879-1899; dashed pink line) *versus* irrigation depleted and dam regulated modern discharges (1970-2004; blue line) at the Port Westward (Beaver) gauge station. Also displayed are: i) 'natural' (dashed black line) *vs* post-dam (solid black line) mean annual discharges and ii) plot of low- and high- river stage water surface profiles. Modified from Naik & Jay (2011). (B) Graph displaying the time averaged potential energy flux divergences of tidal (dashed yellow line) *vs* fluvial (black line) energy sources and mean boundaries of fluvial-tidal transition regimes as predicted by the model of Giese & Jay (1989) and Jay et al. (1990). Modified from Jay et al. (1990).

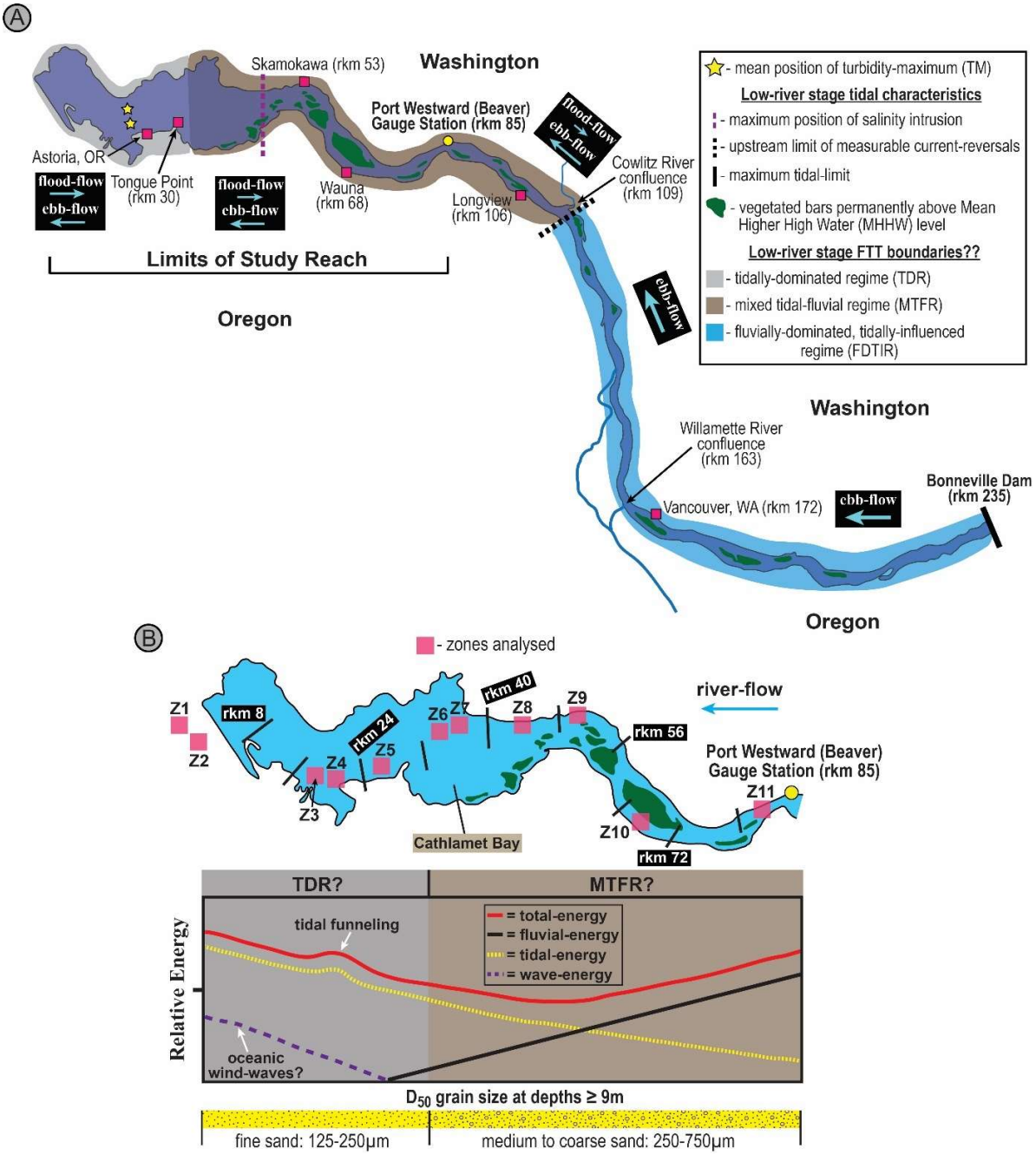

FIGURE 3 (A) Planform diagram of the Lower Columbia River (LCR) from rkm 0-235 displaying the inferred low-river stage boundaries of its fluvial-tidal transition hydraulic regimes as well as the limits and positions of relevant tidal characteristics. (B) Conceptualised low-river stage relative hydrodynamic energy diagram and modern channel bed D_{50} grain size at depths ≥ 9m.

Type-A: ~ rkm 0-9 (tidally-reversing during all river-stages)	
Dune Metric	**Descriptions**
height (η)	~ 0.2-1m
wavelength (λ)	~ 3-10m
aspect ratio (λ/η)	~ 10-20
*symmetry	asymmetric to symmetric
*roundness	commonly not-rounded to sporadically rounded
*dimensionality	2D in planform
*dune type	simple
Type-B: ~ rkm 9-30 (low-discharge ≤ 7,000 m^3s^{-1}); ~ rkm 9-24 (high-discharge > 7,000 m^3s^{-1})	
Dune Metric	**Descriptions**
height (η)	~ 0.3-0.9m
wavelength (λ)	~ 3-40m
aspect ratio (λ/η)	~ 35
*symmetry	asymmetric upstream-oriented (low-flow); asymmetric and downstream-oriented (high-flow)
*roundness	typically not-rounded
*dimensionality	2D in planform
*dune type	simple
Type-C: ~ rkm 30-35 (low-discharge ≤ 7,000 m^3s^{-1}); ~ rkm 24-35 (high-discharge > 7,000 m^3s^{-1})	
Dune Metric	**Descriptions**
height (η)	~ 1-3m
wavelength (λ)	≥ 100m
aspect ratio (λ/η)	~ 50
*symmetry	asymmetric to symmetric, and always downstream-oriented
*roundness	not-rounded to rounded
*dimensionality	3D in planform
*dune type	compound

* = qualitative description provided by reporting authors

TABLE 1 The types and properties of lower Columbia River (LCR) primary dunes (≥ 9m depth; localised H/H_{max} ≥ 0.7) observed by Sherwood & Creager (1990). Dune observations were restricted to between ~ rkm 0-35 and represent a mixture of observations from both high- and low- river stages. See Figure 4A,B for spatial distribution of Type A-C dunes.

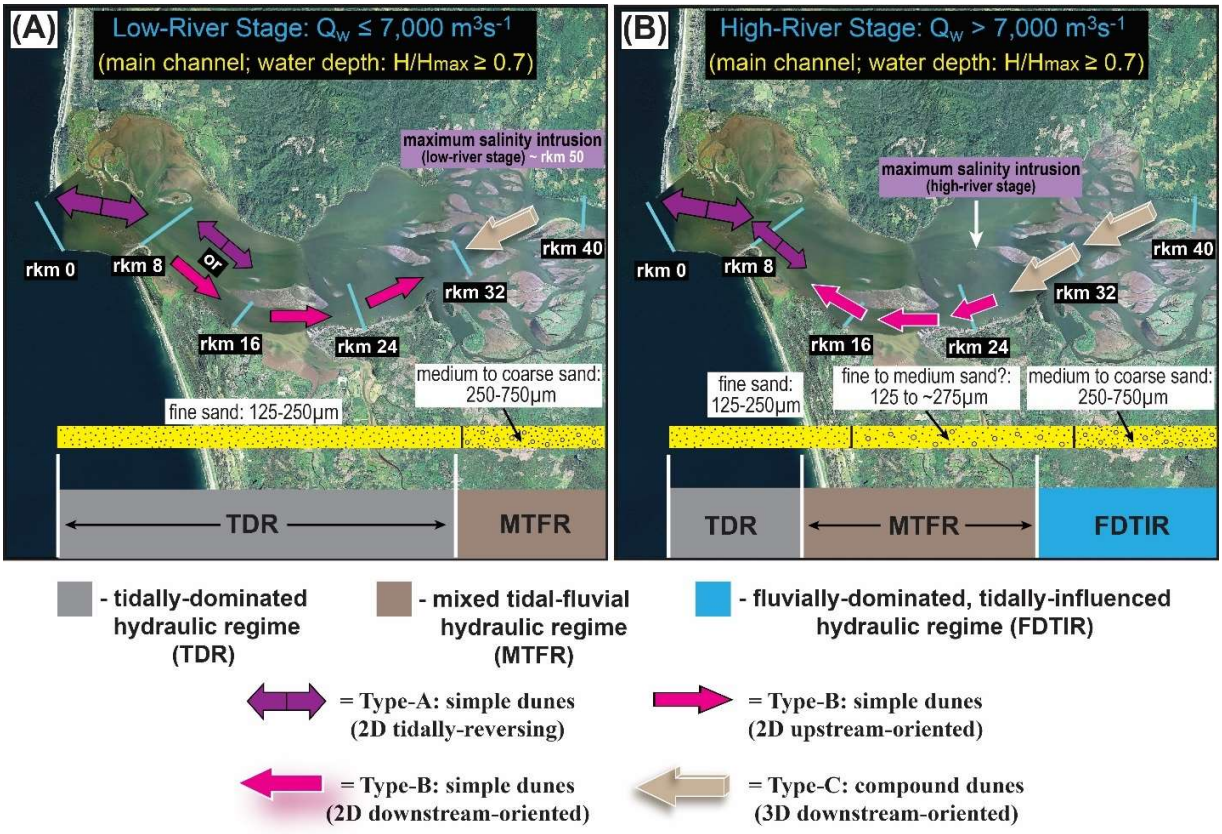

FIGURE 4 Distribution of primary dune morphology (≥ 9m depth; H/H_{max} ≥ 0.7) and channel bed grain size within the main channel of the Lower Columbia River from ~ rkm 0-35 as observed by Sherwood & Creager (1990). Analyses occurred from September 1979 to June 1980 over varying daily and spring-neap tidal-cycles and during (A) low-river stages and (B) high-river stages. Note that fluvial-tidal transition regimes expand and contract as a function of river-stage. See Table 1 and main text for further descriptions of Type-A to C dunes. Adapted from Sherwood & Creager (1990).

Lower Columbia River MBES Channel Reach	Survey Time Interval	Average Fluvial-Discharge Q_{avg} (m^3s^{-1})	Prior Spring Freshet Peak Fluvial-Discharge Q_{wpeak} (m^3s^{-1})
~ **Rkm 0-32** *Z1: ~ 1.0 *Z2: ~ 2.6 †Z3: ~ 18.4 †Z4: ~ 20.9 †Z5: ~ 27.1	Aug. 8th - Oct. 2nd, 2007	~ 3,600	May 5th, 2007: ~ 12,900
~ **Rkm 32-40** ‡Z6: ~ 34.2 ‡Z7: ~ 36.7	Sept. 15th - Sept. 23rd, 2008	~ 4,100	June 6th, 2008: ~ 16,400
~ **Rkm 48-96** ΩZ9: ~ 50.8 ΩZ10: ~ 66.5 ΩZ11: ~ 84.4	Oct. 8th, 2008 - Mar. 5th, 2009	~ 5,300	June 6th, 2008: ~ 16,400
~ **Rkm 40-48** ΦZ8: ~ 44.6	Oct. 7th, 2010 - Jan. 23rd, 2011	~ 6,600	June 13th, 2010: ~ 16,800

* = soundings collected using MBES systems including the Wärtsilä Seabeam/Elac 1180, Klien 5000, and Reson SeaBat 8125 and 8101, deployed amongst multiple vessels

† = soundings collected using MBES systems including the Wärtsilä Seabeam/Elac 1180, and Reson SeaBat 8125 and 8101, deployed between multiple vessels

‡ = soundings collected using MBES systems including the Wärtsilä Seabeam/Elac 1180, and Reson SeaBat 7125, tilted 8125, and 8101, deployed amongst multiple vessels

Ω = soundings collected using Reson SeaBat 7125 and 8101 MBES systems deployed between multiple vessels

Φ = soundings collected using a Kongsberg EM 2002 MBES system deployed on a singular vessel

TABLE 2 Time intervals and average flow-discharges during multi-beam echo sounding (MBES) surveys of the lower Columbia River (LCR) main channel from ~ rkm 0-90 relative to the timing of prior spring freshet peak fluvial-discharge events. Note that prior peak discharges are ~ 2.5-4 times greater than the average discharges during surveying. Included are the approximate river kilometre positions of associated MBES zone(s) where primary dune metrics were quantified. Note that: i) surveying periods for all zones occurred over differing neap-spring and flood-ebb tidal cycles, and ii) differences in vertical soundings between systems were corrected via normalisation to lead-line depth soundings in regions of data overlap. Values of Q_{avg} and Q_{wpeak} were acquired from the Port Westward (Beaver) USGS gauge station (ID: 14246900) positioned at ~ rkm 85.

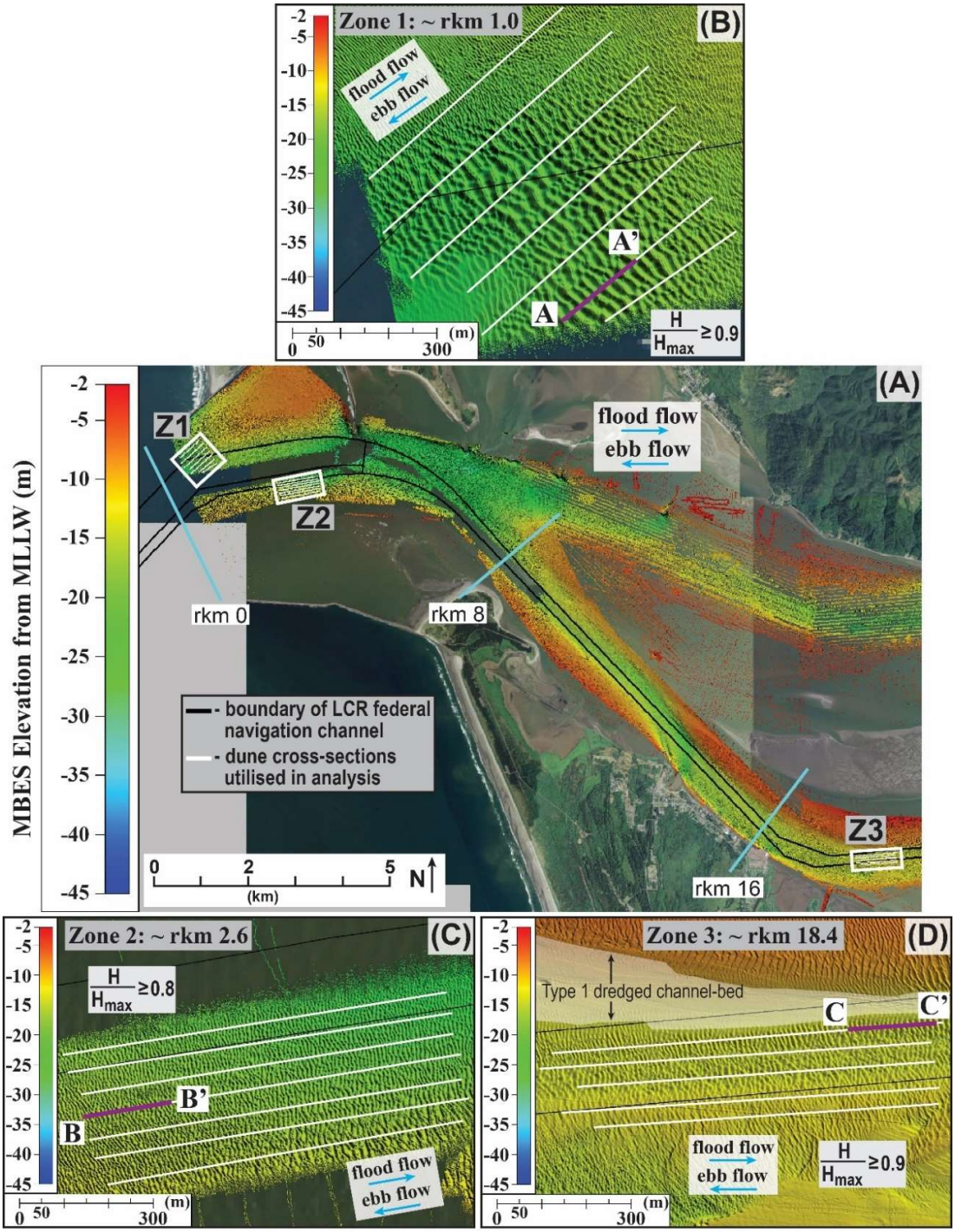

FIGURE 5 (A) Image of the lower Columbia River (LCR) displaying multi-beam echo sounding (MBES) data from ~ rkm 0-19 (zones 1-3; white rectangles) where primary bedforms were analysed with respect to the boundaries of the main navigation channel (black lines). (B-D) Magnified images of zones 1-3 showing the sections (white lines) utilised to quantify bedform metrics. Note that all bedforms examined are 'natural', because they lie outside of Type 1 or 2 dredged regions. See Figure 9 for partial sections A-A' to C-C' (purple lines).

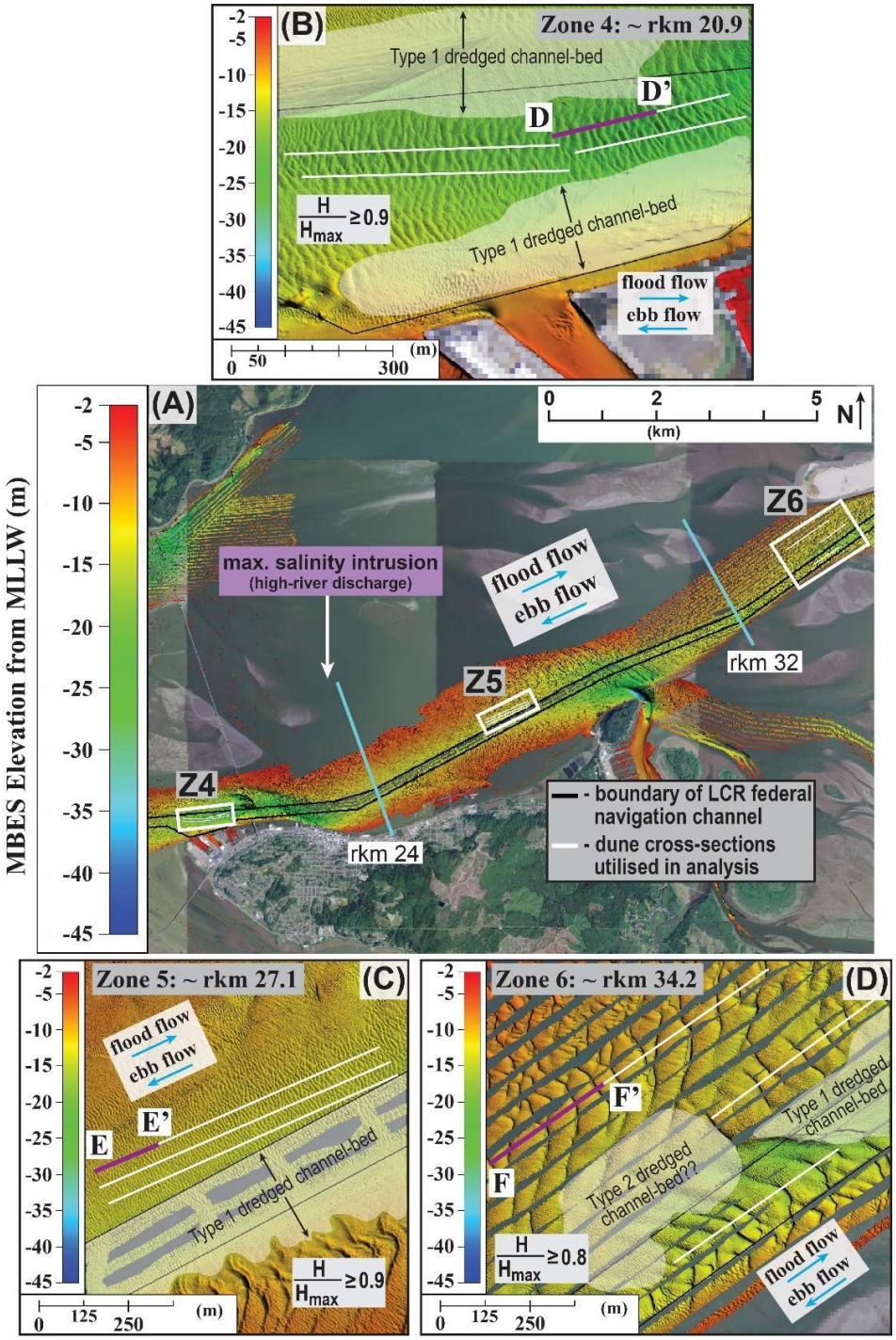

FIGURE 6 (A) Image of the lower Columbia River (LCR) channel reach ranging from ~ rkm 20-35, which displays multi-beam echo sounding (MBES) data of zones 4-6 (white rectangles) where primary bedforms were evaluated. (B-D) Magnified images of zones 4-6 showing the sections (white lines) used to quantify bedform metrics. All bedforms examined are 'natural' because they formed outside of Type 1 or 2 dredged regions. See Figure 9 for partial sections D-D' to F-F' (purple lines).

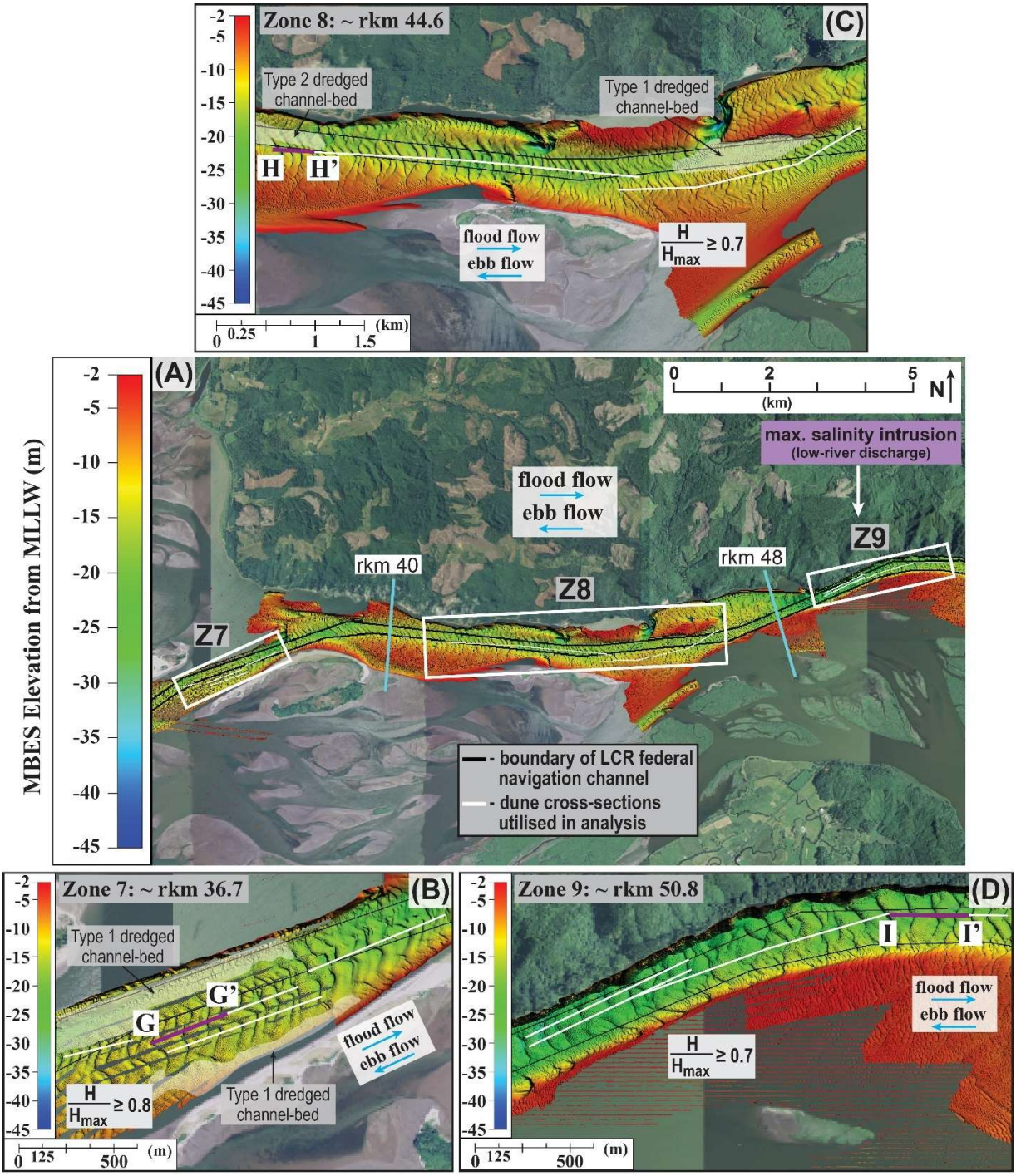

FIGURE 7 (A) Image of the lower Columbia River (LCR) channel reach that encompasses multi-beam echo sounding (MBES) data from ~ rkm 35-52 (zones 7-9; white rectangles) where primary bedforms were examined. (B-D) Magnified images of MBES zones 7-9 displaying the sections (white lines) used to quantify bedform geometric properties. Note that all bedforms analysed exist outside of Type 1 and 2 dredged areas and are therefore 'natural'. Refer to Figure 9 for partial sections G-G' to I-I' (purple lines).

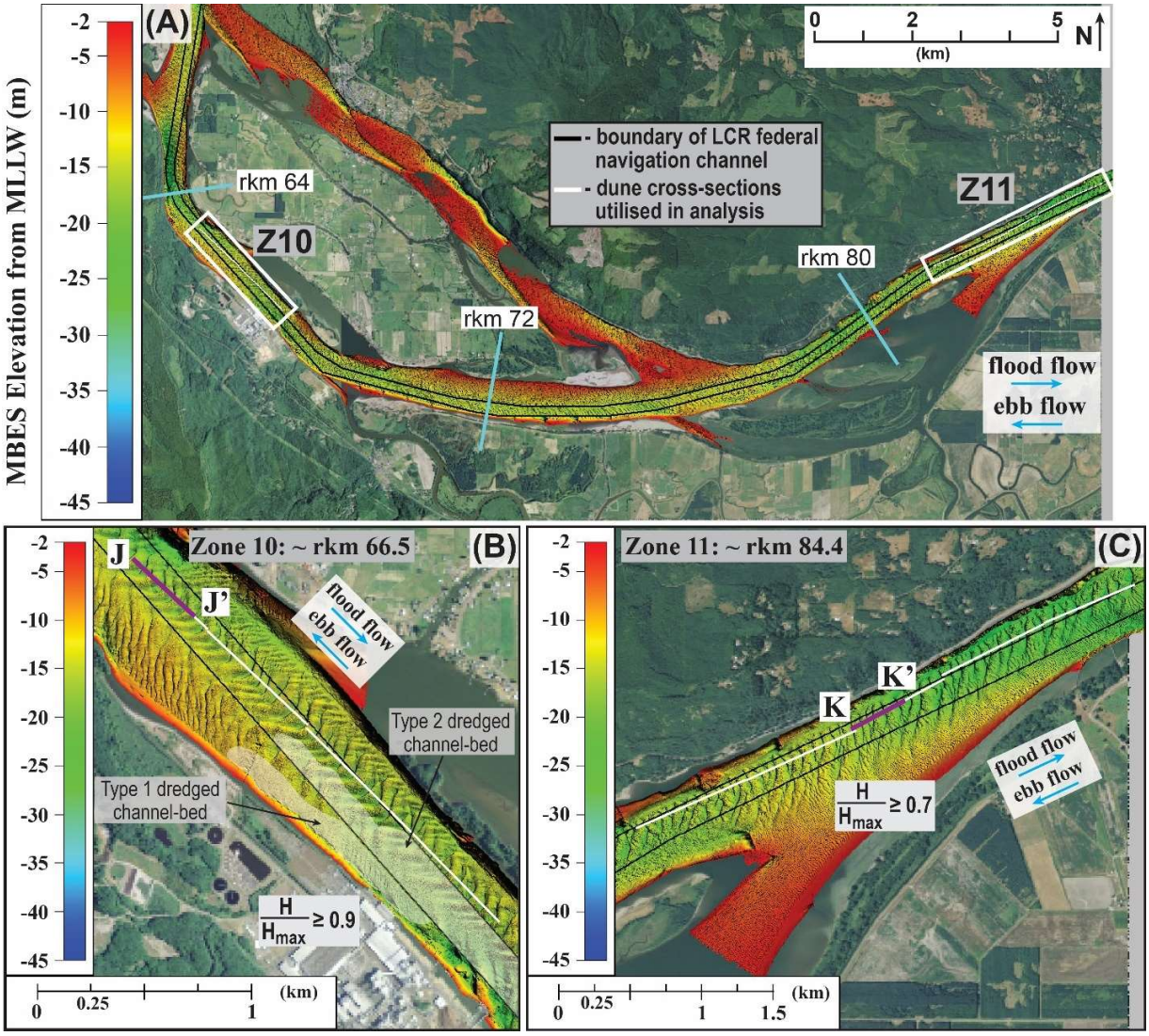

FIGURE 8 (A) Image of the lower Columbia River (LCR) channel reach spanning ~ rkm 60-85 that includes MBES zones 10 and 11 (white rectangles) where primary bedforms were analysed. (B and C) Magnified images of zones 10 and 11 displaying the sections (white lines) used to quantify bedform metrics. Notice that all bedforms investigated are 'natural', because they occur outside of Type 1 or 2 dredged regions. See Figure 9 for partial sections J-J' to K-K' (purple lines).

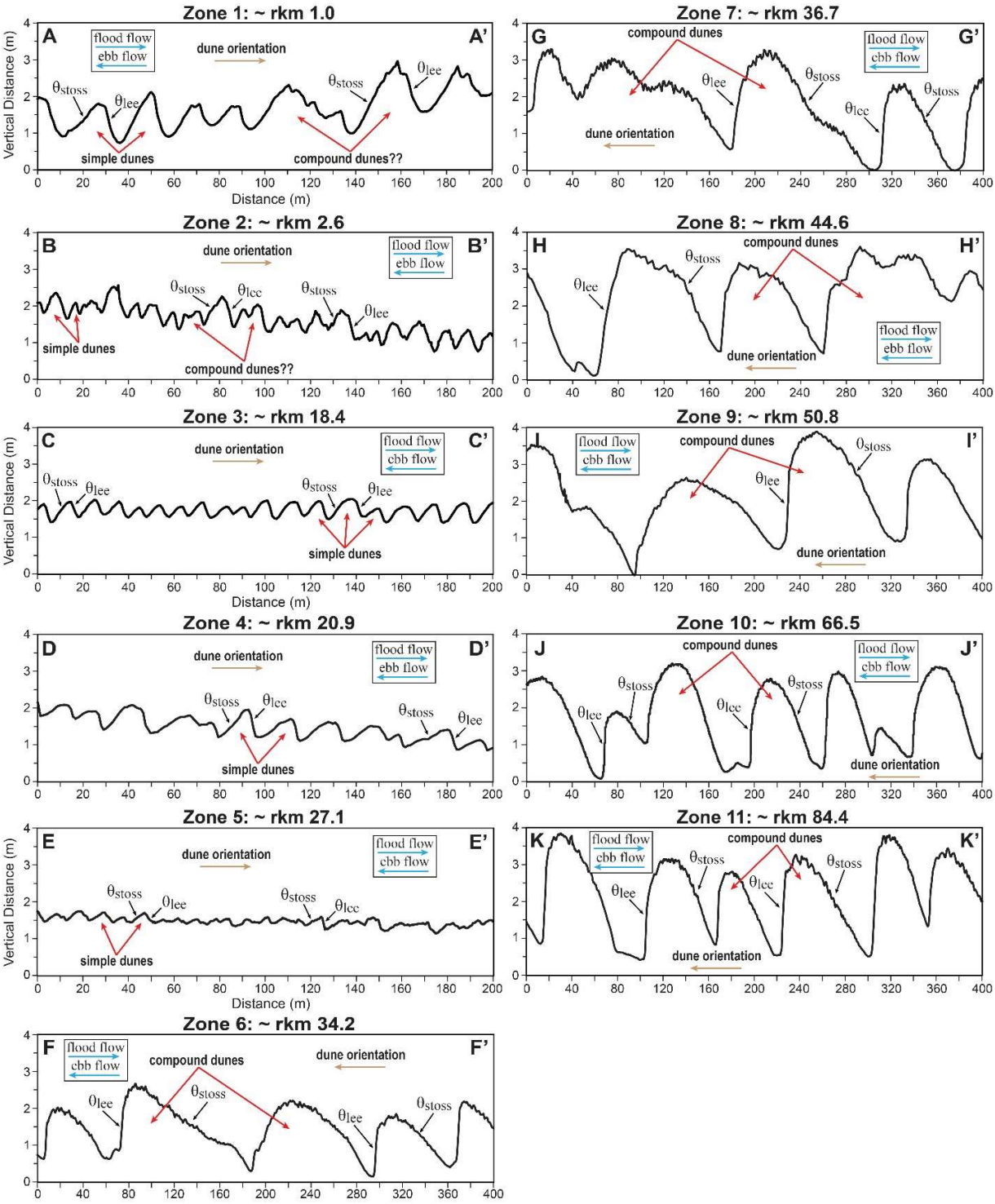

FIGURE 9 Example partial-sections A-A' to K-K' displaying the low-river stage bedform profiles of zones 1-11 (~ rkm 1.0-84.4). The location of individual sections is presented in Figures 5-8 (purple lines).

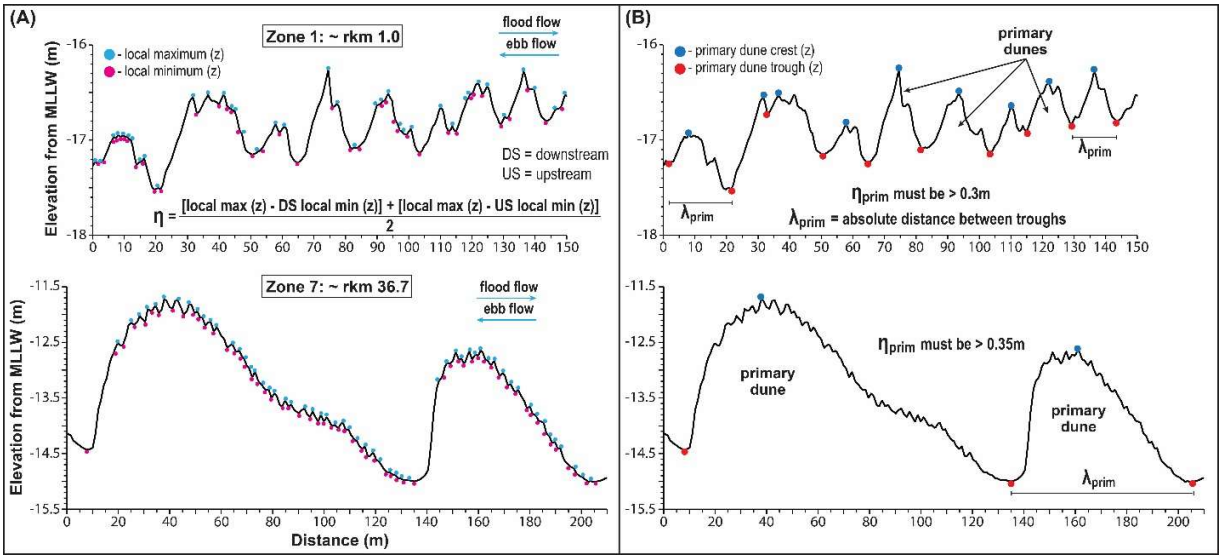

FIGURE 10 (A) Examples of automated measurement technique utilised to identify and compute the heights (η) of all bedforms (both primary and secondary) present in zone sectional profiles. (B) Identification and calculation procedures used to determine only primary dune wavelengths (λ_{prim}) after applying the primary dune height (η_{prim}) cut-offs associated with each zone example in (A). Note that η_{prim} must be greater than the largest η of secondary bedforms present in individual zones. See Table 3 for the primary dune height cut-offs applied to each zone.

LCR MBES Zone	Primary Dune Height Cut-Off (m)
Zone 1: ~ rkm 1.0	$\eta_{prim} > 0.3$
Zone 2: ~ rkm 2.6	$\eta_{prim} > 0.3$
Zone 3: ~ rkm 18.4	$\eta_{prim} > 0.15$
Zone 4: ~ rkm 20.9	$\eta_{prim} > 0.25$
Zone 5: ~ rkm 27.1	$\eta_{prim} > 0.15$
Zone 6: ~ rkm 34.2	$\eta_{prim} > 0.5$
Zone 7: ~ rkm 36.7	$\eta_{prim} > 0.35$
Zone 8: ~ rkm 44.6	$\eta_{prim} > 0.4$
Zone 9: ~ rkm 50.8	$\eta_{prim} > 0.4$
Zone 10: ~ rkm 66.5	$\eta_{prim} > 0.4$
Zone 11: ~ rkm 84.4	$\eta_{prim} > 0.5$

TABLE 3 Primary dune height cut-offs for the eleven zones analysed. Bedforms possessing heights below the reported cut-offs are considered secondary bedforms and were not included in the final distribution of primary dunes whose geometric properties were further characterised.

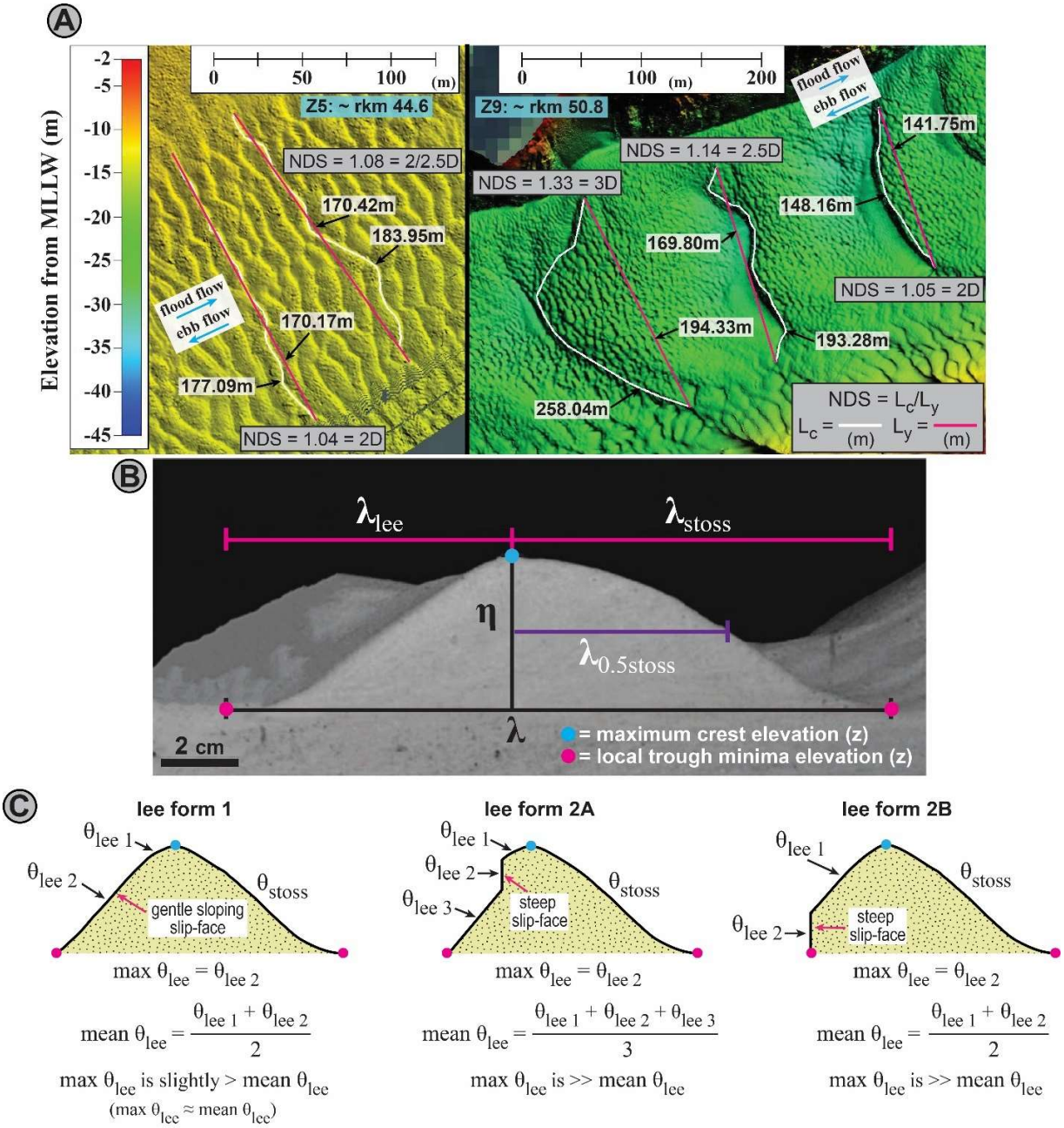

FIGURE 11 (A) Examples of the measurement technique used to calculate the non-dimensional span index, NDS, of primary dunes. See main text for dimensional regime boundaries. (B) Primary dune measurement parameters used in the calculations of bedform symmetry and roundness indices (BSI and BRI). Dune BSI and BRI values were obtained using Equations 3 and 4 . Adapted from Perillo et al. (2014a). (C) Illustrations of the three forms of lee-side morphology present in the primary dunes of the lower Columbia River. Included are example equations and relations used to compute and compare maximum and mean lee-angles of various dune lee forms.

Zone 1: rkm 1.0	Distribution	N	Range	Mean	STD	Median	General Morphology
height (η)	Gamma	113	~ 0.4-1.6m	0.8m	±0.3	0.7m	-
wavelength (λ)	Gamma	113	~ 10-65m	24.3m	±9.0	21.5m	-
aspect ratio (λ/η)	Gamma	113	~ 20-160	34.0	±14.1	28.3	-
BSI	Gamma	113	~ 1-11	1.9	±0.8	1.7	asymmetric
BRI	Gamma	113	~ 0.2-0.7	0.5	±0.1	0.5	not rounded
mean θ_{lee}	Gamma	113	~ 4-16°	8.0°	±2.2	7.7°	LADs
max θ_{lee}	Gamma	113	~ 3-26°	10.9°	±4.4	10.3°	LADs
NDS	Arithmetic	10	1.05-1.11	1.07	±0.02	-	2D
dune form	-	-	-	-	-	-	simple to compound
H_{mean}	-	-	-	20.0m	-	-	-
η_{mean}/H_{mean}	-	-	-	0.04	-	-	-
λ_{mean}/H_{mean}	-	-	-	1.2	-	-	-
Zone 2: rkm 2.6	Distribution	N	Range	Mean	STD	Median	General Morphology
height (η)	Gamma	444	~ 0.3-1.3m	0.6m	±0.1	0.5m	-
wavelength (λ)	Gamma	444	~ 5-40m	13.1m	±5.4	11.2m	-
aspect ratio (λ/η)	Gamma	444	~ 10-95	24.0	±9.2	20.1	-
BSI	Gamma	444	~ 1-6	1.9	±0.8	1.5	asymmetric
BRI	Gamma	444	~ 0.2-0.9	0.5	±0.1	0.5	not rounded
mean θ_{lee}	Gamma	444	~ 6-20°	10.8°	±2.7	10.4°	LADs
max θ_{lee}	Gamma	444	~ 5-33°	14.6°	±5.5	13.8°	LADs
NDS	Arithmetic	12	1.02-1.05	1.05	±0.01	-	2D
dune form	-	-	-	-	-	-	simple to compound
H_{mean}	-	-	-	18.4m	-	-	-
η_{mean}/H_{mean}	-	-	-	0.03	-	-	-
λ_{mean}/H_{mean}	-	-	-	0.7	-	-	-
Zone 3: rkm 18.4	Distribution	N	Range	Mean	STD	Median	General Morphology
height (η)	Gamma	309	~ 0.2-0.7m	0.4m	±0.1	0.4m	-
wavelength (λ)	Gamma	309	~ 2-50m	13.2m	±4.8	11.7m	-
aspect ratio (λ/η)	Gamma	309	~ 20-160	39.0	±16.1	32.0	-
BSI	Gamma	309	~ 1-8	1.9	±0.7	1.7	asymmetric
BRI	Gamma	309	~ 0.2-0.8	0.5	±0.1	0.5	not rounded
mean θ_{lee}	Gamma	309	~ 5-13°	7.3°	±1.5	7.2°	LADs
max θ_{lee}	Gamma	309	~ 4-21°	10.2°	±3.1	9.9°	LADs
NDS	Arithmetic	44	1.02-1.21	1.08	±0.04	-	2/2.5D
dune form	-	-	-	-	-	-	simple
H_{mean}	-	-	-	14.4m	-	-	-
η_{mean}/H_{mean}	-	-	-	0.03	-	-	-
λ_{mean}/H_{mean}	-	-	-	0.9	-	-	-

Table 4 continued.

Zone 4: rkm 20.9	Distribution	N	Range	Mean	STD	Median	General Morphology
height (η)	Gamma	70	~ 0.3-0.8m	0.5m	±0.1	0.5m	-
wavelength (λ)	Gamma	70	~ 10-50m	22.0m	±7.1	21.2m	-
aspect ratio (λ/η)	Gamma	70	~ 30-150	46.1	±15.8	40.9	-
BSI	Gamma	70	~ 1-10	2.5	±1.3	2.1	asymmetric
BRI	Gamma	70	~ 0.3-0.8	0.5	±0.1	0.5	not rounded
mean θ_{lee}	Gamma	70	~ 5-15°	9.6°	±2.4	9.2°	LADs
max θ_{lee}	Gamma	70	~ 6-25°	14.4°	±4.8	13.6°	LADs
NDS	Arithmetic	12	1.05-1.15	1.08	±0.03	-	2/2.5D
dune form	-	-	-	-	-	-	simple
H_{mean}	-	-	-	19.4m	-	-	-
η_{mean}/H_{mean}	-	-	-	0.03	-	-	-
λ_{mean}/H_{mean}	-	-	-	1.1	-	-	-
Zone 5: rkm 27.1	Distribution	N	Range	Mean	STD	Median	General Morphology
height (η)	Gamma	222	~ 0.2-0.5m	0.3m	±0.1	0.2m	-
wavelength (λ)	Gamma	222	~ 10-110m	16.0m	±7.9	12.1m	-
aspect ratio (λ/η)	Gamma	222	~ 50-450	67.5	±37.6	50.5	-
BSI	Gamma	222	~ 2-22	2.6	±1.5	2.1	asymmetric
BRI	Gamma	222	~ 0.2-0.8	0.6	±0.1	0.6	not rounded
mean θ_{lee}	Gamma	222	~ 4-13°	7.1°	±1.9	6.8°	LADs
max θ_{lee}	Gamma	222	~ 4-22°	10.9°	±3.7	10.2°	LADs
NDS	Arithmetic	12	1.03-1.09	1.05	±0.02	-	2D
dune form	-	-	-	-	-	-	simple
H_{mean}	-	-	-	13.8m	-	-	-
η_{mean}/H_{mean}	-	-	-	0.02	-	-	-
λ_{mean}/H_{mean}	-	-	-	1.2	-	-	-
Zone 6: rkm 34.2	Distribution	N	Range	Mean	STD	Median	General Morphology
height (η)	Gamma	22	~ 0.6-2.1m	1.6m	±0.4	1.6m	-
wavelength (λ)	Gamma	22	~ 45-125m	85.0m	±23.7	82.4m	-
aspect ratio (λ/η)	Gamma	22	~ 35-95	54.9	±15.4	52.8	-
BSI	Gamma	22	~ 1-7	2.7	±1.4	2.0	asymmetric
BRI	Gamma	22	~ 0.3-0.7	0.6	±0.10	0.6	not rounded
mean θ_{lee}	Gamma	22	~ 7-20°	13.5°	±3.9	13.9°	LADs
max θ_{lee}	Gamma	22	~ 10-36°	23.0°	±7.7	23.9°	LADs
NDS	Arithmetic	6	1.10-1.33	1.22	±0.1	-	3D
dune form	-	-	-	-	-	-	compound
H_{mean}	-	-	-	13.7m	-	-	-
η_{mean}/H_{mean}	-	-	-	0.12	-	-	-
λ_{mean}/H_{mean}	-	-	-	6.2	-	-	-

Table 4 continued.

Zone 7: rkm 36.7	Distribution	N	Range	Mean	STD	Median	General Morphology
height (η)	Gamma	44	~ 0.5-4m	2.0m	±0.8	2.1m	-
wavelength (λ)	Gamma	44	~ 20-130m	76.0m	±30.7	72.0m	-
aspect ratio (λ/η)	Gamma	44	~ 20-85	38.6	±12.0	37.4	-
BSI	Gamma	44	~ 1-4.3	2.2	±0.8	2.0	asymmetric
BRI	Gamma	44	~ 0.4-0.8	0.6	±0.1	0.6	not rounded
mean θ_{lee}	Gamma	44	~ 4-19°	12.1°	±4.3	12.6°	LADs
max θ_{lee}	Gamma	44	~ 4-32°	19.4°	±8.6	20.4°	LADs
NDS	Arithmetic	14	1.07-1.33	1.20	±0.08	-	3D
dune form	-	-	-	-	-	-	compound
H_{mean}	-	-	-	16.1m	-	-	-
η_{mean}/H_{mean}	-	-	-	0.13	-	-	-
λ_{mean}/H_{mean}	-	-	-	4.7	-	-	-
Zone 8: rkm 44.6	Distribution	N	Range	Mean	STD	Median	General Morphology
height (η)	Gamma	50	~ 1-4m	1.9m	±0.7	1.8m	-
wavelength (λ)	Gamma	50	~ 30-170m	74.3m	±25.4	73.3m	-
aspect ratio (λ/η)	Gamma	50	~ 25-85	41.4	±12.7	38.9	-
BSI	Gamma	50	~ 1.2-3.7	2.0	±0.7	1.8	asymmetric
BRI	Gamma	50	~ 0.3-0.7	0.6	±0.1	0.6	not rounded
mean θ_{lee}	Gamma	50	~ 4-17°	11.3°	±3.6	9.2°	LADs
max θ_{lee}	Gamma	50	~ 4-30°	18.2°	±7.2	18.8°	LADs
NDS	Arithmetic	19	1.07-1.51	1.17	±0.09	-	3D
dune type	-	-	-	-	-	-	Compound
H_{mean}	-	-	-	15.7m	-	-	-
η_{mean}/H_{mean}	-	-	-	0.12	-	-	-
λ_{mean}/H_{mean}	-	-	-	4.7	-	-	-
Zone 9: rkm 50.8	Distribution	N	Range	Mean	STD	Median	General Morphology
height (η)	Gamma	34	~ 0.8-4.5m	2.5m	±1.0	2.4m	-
wavelength (λ)	Gamma	34	~ 30-160m	109.7m	±40.0	114.7m	-
aspect ratio (λ/η)	Gamma	34	~ 30-120	48.3	±17.8	40.9	-
BSI	Gamma	34	~ 1-3.5	1.9	±0.6	1.9	asymmetric
BRI	Gamma	34	~ 0.4-0.7	0.6	±0.1	0.6	not rounded
mean θ_{lee}	Gamma	34	~ 7-21°	13.2°	±3.6	12.8°	LADs
max θ_{lee}	Gamma	34	~ 12-36°	23.8°	±6.3	23.2°	LADs
NDS	Arithmetic	16	1.05-1.33	1.17	±0.09	-	3D
dune type	-	-	-	-	-	-	compound
H_{mean}	-	-	-	24.0m	-	-	-
η_{mean}/H_{mean}	-	-	-	0.10	-	-	-
λ_{mean}/H_{mean}	-	-	-	4.6	-	-	-

Table 4 continued.

Zone 10: rkm 66.5	Distribution	N	Range	Mean	STD	Median	General Morphology
height (η)	Gamma	34	~ 0.8-3.3m	2.0m	±0.8	2.2m	-
wavelength (λ)	Gamma	34	~ 20-100m	60.5m	±21.5	57.4m	-
aspect ratio (λ/η)	Gamma	34	~ 20-50	31.0	±7.6	29.9	-
BSI	Gamma	34	~ 1-4.5	2.2	±0.7	2.1	asymmetric
BRI	Gamma	34	~ 0.3-0.7	0.6	±0.1	0.6	not rounded
mean θ_{lee}	Gamma	34	~ 6-20°	14.5°	±3.4	15.4°	LADs
max θ_{lee}	Gamma	34	~ 9-36°	25.3°	±6.3	26.2°	HADs
NDS	Arithmetic	13	1.18-1.28	1.22	±0.04	-	3D
dune type	-	-	-	-	-	-	compound
H_{mean}	-	-	-	16.2m	-	-	-
η_{mean}/H_{mean}	-	-	-	0.13	-	-	-
λ_{mean}/H_{mean}	-	-	-	3.7	-	-	-
Zone 11: rkm 84.4	Distribution	N	Range	Mean	STD	Median	General Morphology
height (η)	Gamma	46	~ 0.8-5m	3.0m	±1.1	2.9m	-
wavelength (λ)	Gamma	46	~ 30-140m	74.9m	±23.2	72.0m	-
aspect ratio (λ/η)	Gamma	46	~ 15-55	26.8	±7.8	24.9	-
BSI	Gamma	46	~ 1.5-6.5	3.0	±1.1	2.6	asymmetric
BRI	Gamma	46	~ 0.4-0.7	0.5	±0.1	0.5	not rounded
mean θ_{lee}	Gamma	46	~ 8-33°	17.7°	±5.2	17.1°	LADs
max θ_{lee}	Gamma	46	~ 13-34°	29.1°	±4.6	29.9°	HADs
NDS	Arithmetic	18	1.05-1.25	1.11	±0.05	-	2.5D
dune type	-	-	-	-	-	-	compound
H_{mean}	-	-	-	19.1m	-	-	-
η_{mean}/H_{mean}	-	-	-	0.15	-	-	-
λ_{mean}/H_{mean}	-	-	-	3.9	-	-	-

TABLE 4 Primary dune (≥ 9m depth; local H/H_{max} ≥ 0.7) characteristics throughout the fluvial-tidal transition of the lower Columbia River at low-river discharge. Standard deviations (STD) are at ± one σ from mean values. Note that zones within the tidally-dominated and mixed tidal-fluvial regimes are highlighted in grey and tan, respectively.

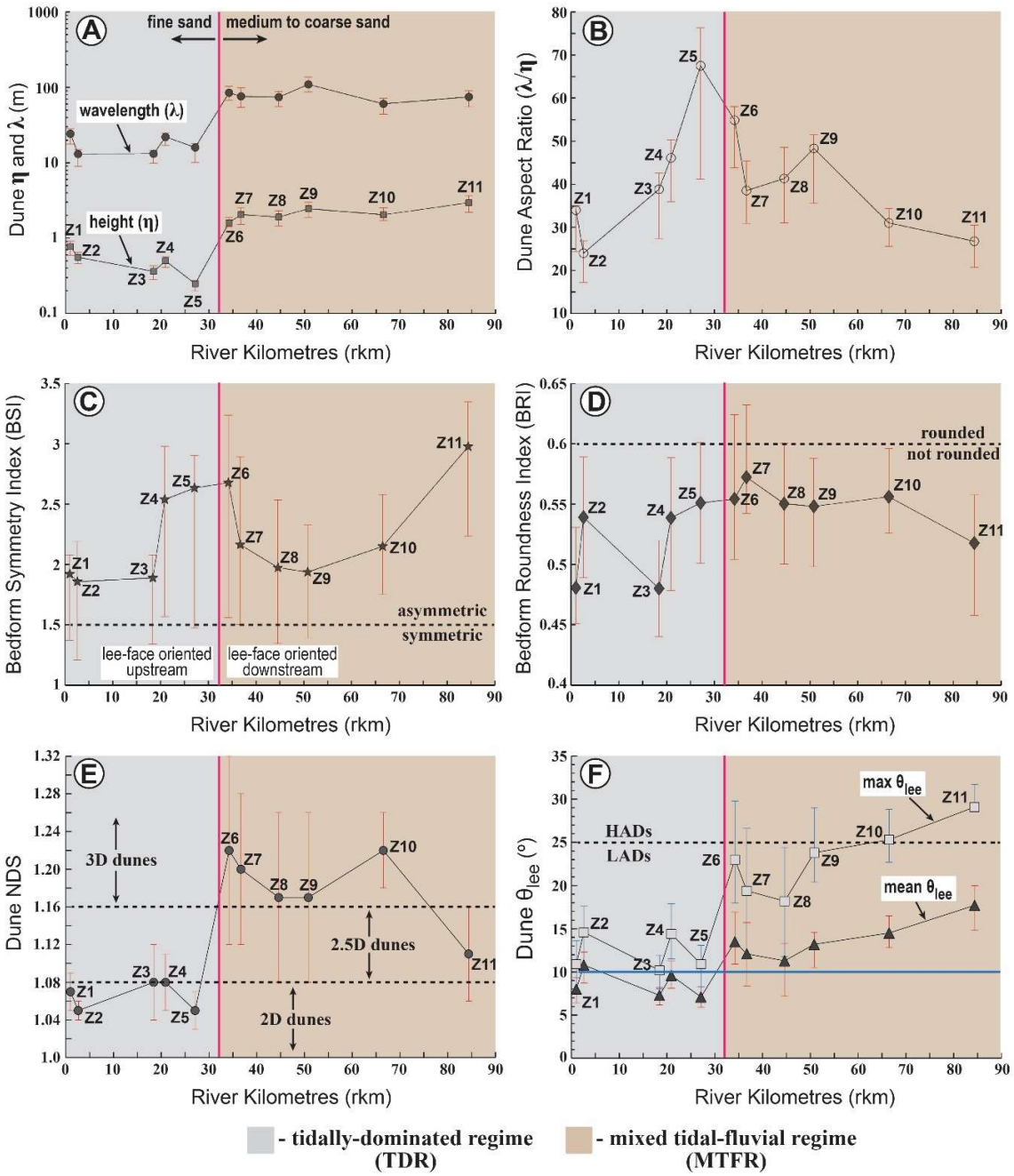

FIGURE 12 (A-F) Mean primary dune (≥ 9m depth; local H/H_{max} ≥ 0.7) characteristics throughout the fluvial-tidal transition of the lower Columbia River (LCR) at low-river stage. For (A-D) and (F), reported mean values are bracketed by error bars extending from the 25th to 75th quartiles of their gamma distributions, whilst in (E) error bars represent values at ± one σ from the arithmetic mean. The vertical pink solid line in (A-F) marks the transition between dunes composed of fine sand that are upstream oriented (below ~ rkm 32) and those composed of medium to coarse sand that are downstream oriented (above ~ rkm 32). The horizontal blue solid line in (F) denotes the mean θ_{lee} (~ 10°) of both deep (≥ 2.5m depth), rivers (Cisneros et al., 2020) and estuarine dunes (Dalrymple & Rhodes, 1995).

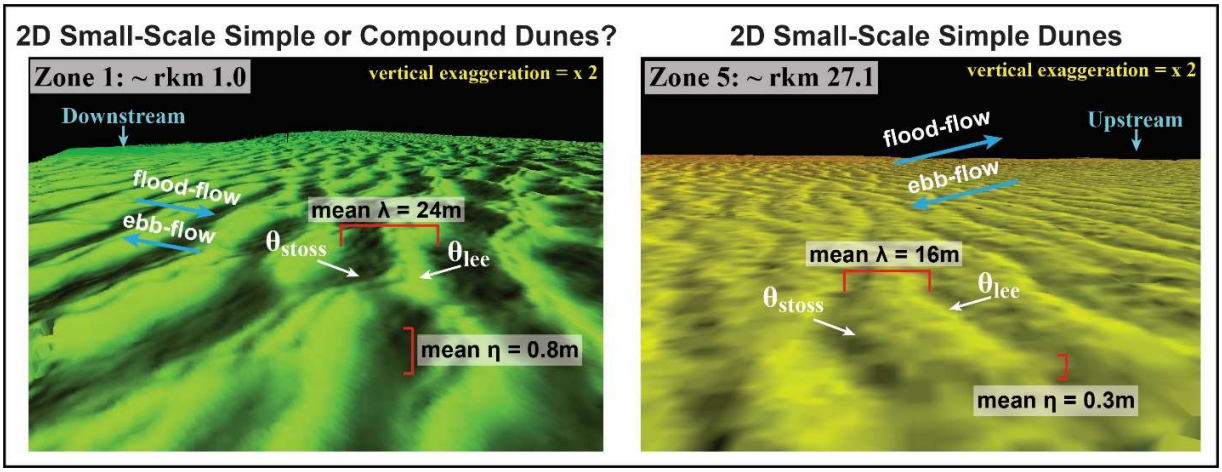

FIGURE 13 Examples of low-angle dunes of the tidally-dominated regime (TDR) at low-fluvial discharge (< 7,000 m^3s^{-1}).

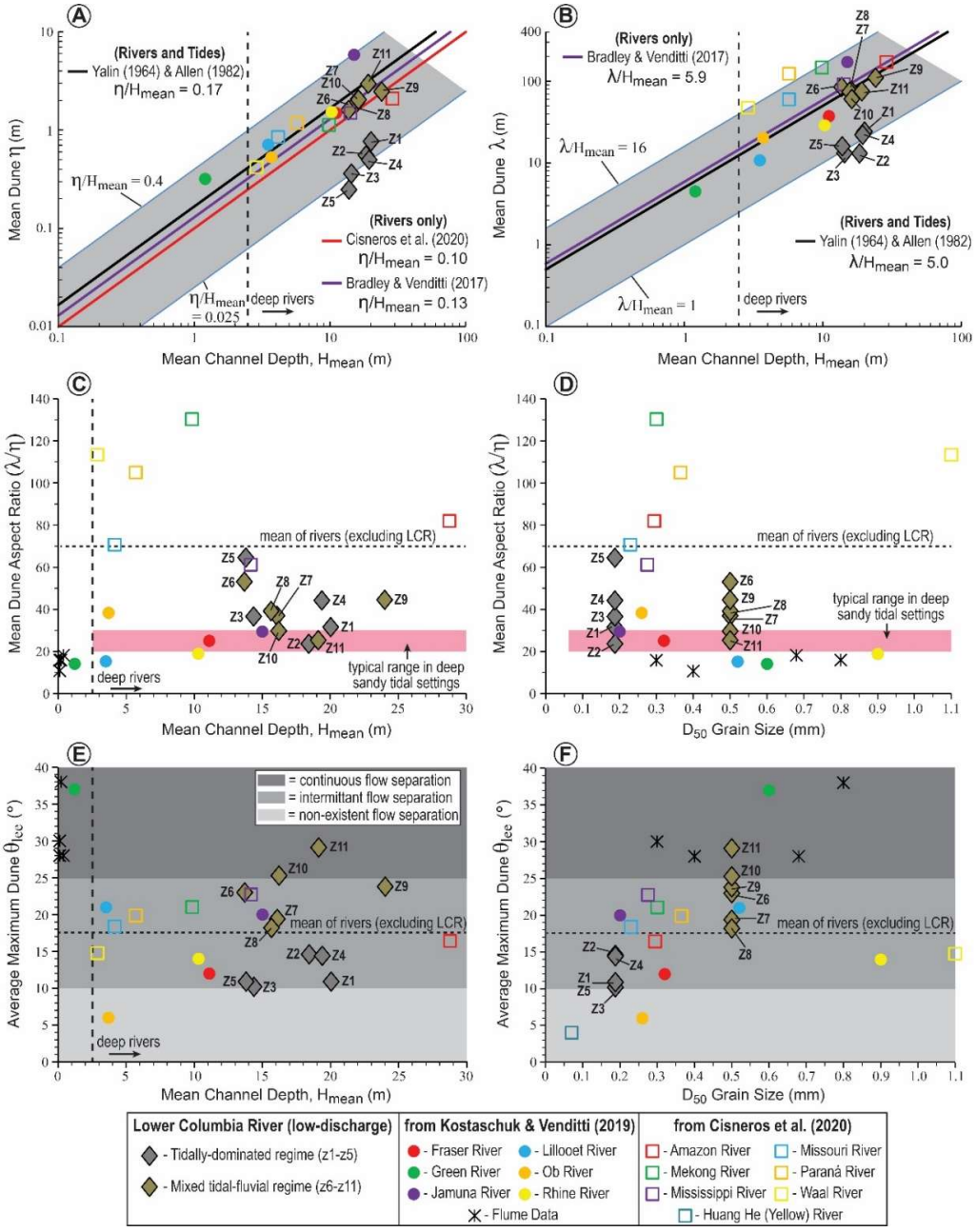

FIGURE 14 (A-B) Mean height (η) and wavelength (λ) scaling relations for the primary dunes (≥ 9m depth; local H/H_{max} ≥ 0.7) of the fluvial-tidal transition of the lower Columbia River as a function of mean channel depth (H_{mean}) relative to other fluvial (coloured circles and open squares) and estuarine environments (note that the grey shaded region bounds the scatter of data for both fluvial and tidal-estuarine settings). (C-D) Comparisons of fluvial-tidal transition dune aspect ratios versus depth and grain size relative to those of other fluvial, flume, and estuarine settings. (E-F) Plots of fluvial-tidal transition dune maximum lee-angles versus those of other rivers and unidirectional flume experiments as a function of channel depth and grain size.

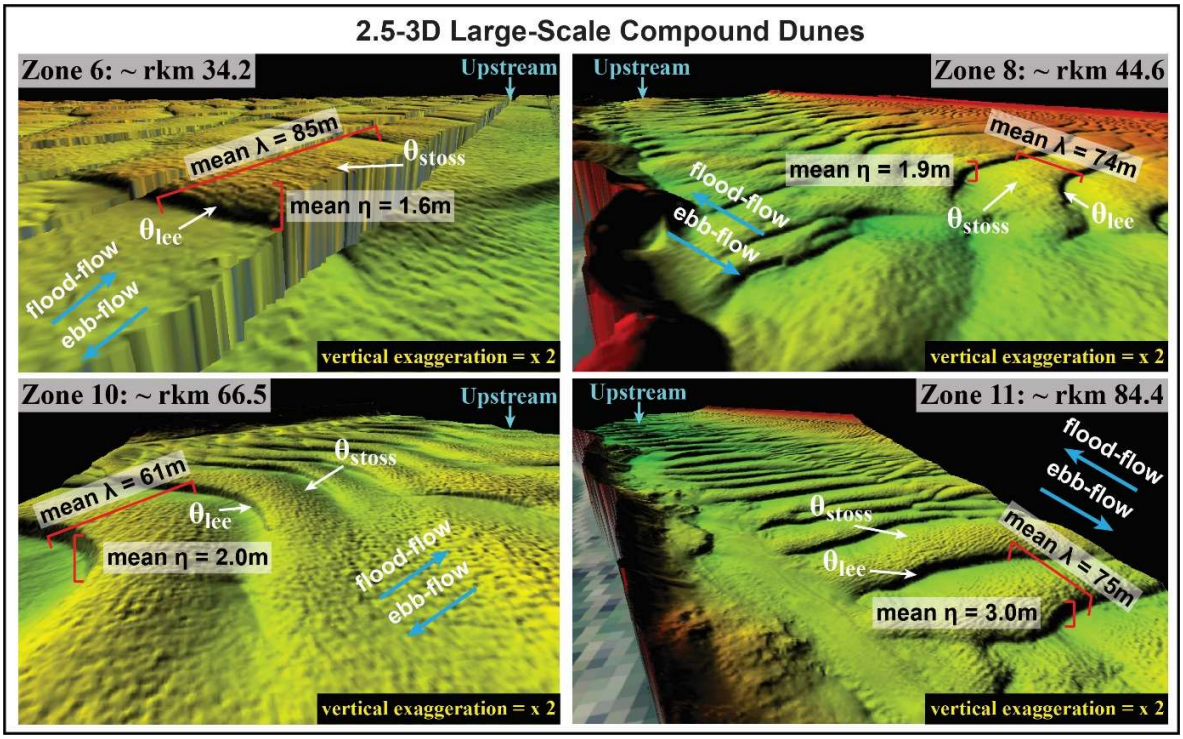

FIGURE 15 Examples of the compound dunes within the mixed tidal-fluvial regime at low-fluvial discharge (< 7,000 m^3s^{-1}).

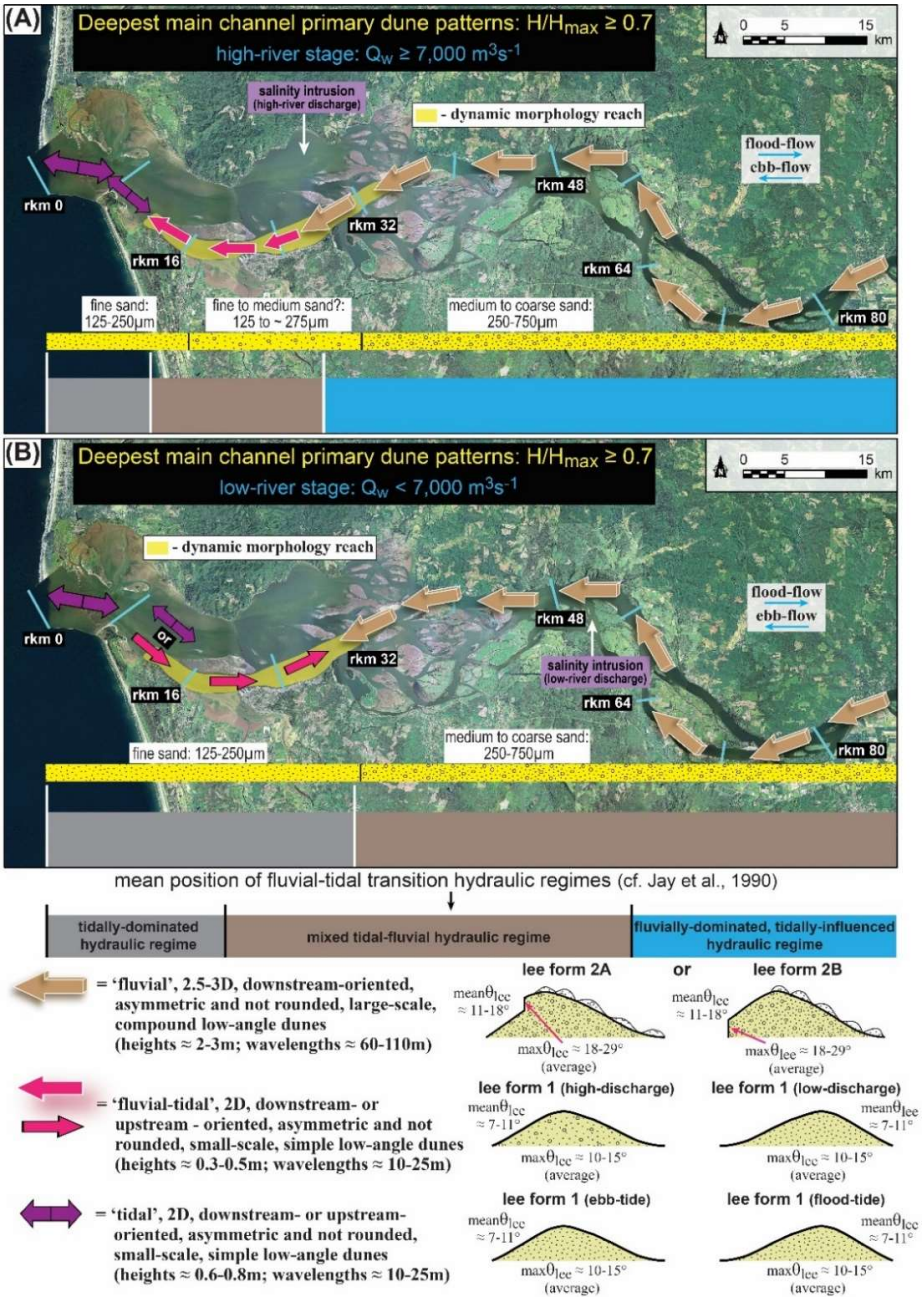

FIGURE 16 Comparison of fluvial-tidal transition primary dune morphology (≥ 9m depth; local H/H_{max} ≥ 0.7) patterns and distributions at Lower Columbia River: (A) high-river stage, and (B) low-river stage. 'Fluvial' dunes dominate throughout the fluvial-tidal transition (~86-90% of total), whilst 'fluvial-tidal to tidal' dunes are only present in the most seaward portions (~ 10-14% of total). Changes between high- and low- fluvial flows drives the expansion and contraction of its fluvial-tidal transition hydraulic regimes, which leads to the development of a 'dynamic morphology reach' (~ rkm 12-35; highlighted in yellow) that experiences the greatest spatio-temporal variance in primary dune morphology. Results represent the integration of the findings from this study and those of Sherwood & Creager (1990) presented in Figure 4A, B.